



Optimizing Cadences with Realistic Light-curve Filtering for Serendipitous Kilonova Discovery with Vera Rubin Observatory

Igor Andreoni¹, Michael W. Coughlin², Mouza Almualla³, Eric C. Bellm⁴, Federica B. Bianco^{5,6,7}, Mattia Bulla⁸, Antonino Cucchiara⁹, Tim Dietrich^{10,11}, Ariel Goobar¹², Erik C. Kool⁸, Xiaolong Li⁵, Fabio Ragosta¹³, Ana Sagués-Carracedo¹², and Leo P. Singer^{14,15}

¹ Division of Physics, Mathematics and Astronomy, California Institute of Technology, Pasadena, CA 91125, USA; andreoni@umd.edu

² School of Physics and Astronomy, University of Minnesota, Minneapolis, MN 55455, USA

³ Department of Physics, American University of Sharjah, PO Box 26666, Sharjah, UAE

⁴ DIRAC Institute, Department of Astronomy, University of Washington, 3910 15th Avenue NE, Seattle, WA 98195, USA

⁵ Department of Physics and Astronomy, University of Delaware, Newark, DE, 19716, USA

⁶ Joseph R. Biden, Jr., School of Public Policy and Administration, University of Delaware, Newark, DE, 19716, USA

⁷ Data Science Institute, University of Delaware, Newark, DE, 19716, USA

⁸ The Oskar Klein Centre, Department of Astronomy, Stockholm University, AlbaNova, SE-106 91 Stockholm, Sweden

⁹ College of Marin, 120 Kent Avenue, Kentfield 94904 CA, USA

¹⁰ Institut für Physik und Astronomie, Universität Potsdam, D-14476 Potsdam, Germany

¹¹ Max Planck Institute for Gravitational Physics (Albert Einstein Institute), Am Mühlenberg 1, Potsdam D-14476, Germany

¹² The Oskar Klein Centre, Department of Physics, Stockholm University, AlbaNova, SE-106 91 Stockholm, Sweden

¹³ INAF-Osservatorio Astronomico di Capodimonte, via Moiariello 16, I-80131, Naples, Italy

¹⁴ Astrophysics Science Division, NASA Goddard Space Flight Center, MC 661, Greenbelt, MD 20771, USA

¹⁵ Joint Space-Science Institute, University of Maryland, College Park, MD 20742, USA

Received 2021 June 12; revised 2021 July 22; accepted 2021 July 26; published 2021 December 22

Abstract

Current and future optical and near-infrared wide-field surveys have the potential to find kilonovae, the optical and infrared counterparts to neutron star mergers, independently of gravitational-wave or high-energy gamma-ray burst triggers. The ability to discover fast and faint transients such as kilonovae largely depends on the area observed, the depth of those observations, the number of revisits per field in a given time frame, and the filters adopted by the survey; it also depends on the ability to perform rapid follow-up observations to confirm the nature of the transients. In this work, we assess kilonova detectability in existing simulations of the Legacy Survey of Space and Time strategy for the Vera C. Rubin Wide Fast Deep survey, with focus on comparing rolling to baseline cadences. Although currently available cadences can enable the detection of >300 kilonovae out to ~ 1400 Mpc over the 10 year survey, we can expect only 3–32 kilonovae similar to GW170817 to be recognizable as fast-evolving transients. We also explore the detectability of kilonovae over the plausible parameter space, focusing on viewing angle and ejecta masses. We find that observations in redder *izy* bands are crucial for identification of nearby (within 300 Mpc) kilonovae that could be spectroscopically classified more easily than more distant sources. Rubin’s potential for serendipitous kilonova discovery could be increased by gain of efficiency with the employment of individual 30 s exposures (as opposed to 2×15 s snap pairs), with the addition of red-band observations coupled with same-night observations in *g* or *r* bands, and possibly with further development of a new rolling-cadence strategy.

Unified Astronomy Thesaurus concepts: [Transient detection \(1957\)](#); [Transient sources \(1851\)](#); [Neutron stars \(1108\)](#); [Gravitational wave sources \(677\)](#); [Surveys \(1671\)](#); [Optical astronomy \(1776\)](#)

1. Introduction

Binary neutron star (BNS) and neutron star–black hole (NSBH) mergers have long been predicted to be associated with short gamma-ray bursts (GRBs; e.g., Blinnikov et al. 1984), and optical/infrared transients called kilonovae (e.g., Li & Paczyński 1998). Along with claimed evidence for kilonovae in some short GRBs (e.g., Berger et al. 2013; Tanvir et al. 2013; Lamb et al. 2019; Jin et al. 2020), the discovery of a kilonova (e.g., Coulter et al. 2017) associated with the first BNS merger detected in gravitational waves, GW170817 (Abbott et al. 2017b), nicely confirmed these predictions. This multimessenger source marked a watershed moment in astrophysics, with prospects to strongly constrain both the

neutron star equation of state (e.g., Metzger 2017; Annala et al. 2018; Radice et al. 2018; Most et al. 2018; Tews et al. 2018; Radice & Dai 2019; Essick et al. 2020; Capano et al. 2020; Dietrich et al. 2020) and the Hubble Constant (e.g., Abbott et al. 2017a; Hotokezaka et al. 2018; Fishbach et al. 2019; Coughlin et al. 2020; Dhawan et al. 2020; Dietrich et al. 2020), among many other science cases including cosmological gravity (Baker et al. 2017) and dark energy (Ezquiaga & Zumalacárregui 2017).

Dynamical ejecta (e.g., Bauswein et al. 2013; Hotokezaka et al. 2013; Dietrich & Ujevic 2017), which arise from tidal stripping of the neutron star(s) and the neutron star’s contact interface, and postmerger ejecta (e.g., Metzger et al. 2008; Fernández et al. 2015; Siegel & Metzger 2018; Fernández et al. 2019), which arise from accretion disk winds surrounding the remnant object, are characterized by low electron fractions. This scenario favors the production of heavy elements such as lanthanides and actinides via rapid neutron capture (known as the *r*-process), and the decay

of these unstable nuclei powers the optical/infrared kilonova (e.g., Lattimer & Schramm 1974; Barnes & Kasen 2013; Kasen et al. 2013; Barnes et al. 2016; Kasen et al. 2017).

Questions about the sources of heavy element production in the universe and diversity in the ejecta of the kilonova population can only be answered by the detection and characterization of a large sample of sources. Unveiling such a population is difficult because kilonovae are rare ($<1\%$ of the core-collapse supernova rate), fast (fading $\gtrsim 0.5$ mag per day in the optical), and faint transients ($M \gtrsim -16$ at peak), and hence are particularly hard to discover. Signatures of kilonovae are mostly found during the follow-up of short GRBs (e.g., Perley et al. 2009) and the follow-up of LIGO/Virgo candidates, although only for GW170817 has a counterpart been identified so far (e.g., Andreoni et al. 2017; Arcavi et al. 2017; Cowperthwaite et al. 2017; Kasliwal et al. 2017; Pian et al. 2017; Smartt et al. 2017). Rates of BNS mergers are still highly uncertain, with $R = 80\text{--}810 \text{ Gpc}^{-3} \text{ yr}^{-1}$ based on gravitational-wave observations (The LIGO Scientific Collaboration et al. 2021); empirical limits on kilonovae rates by optical surveys are nearing the upper end of the gravitational-wave measurements (Andreoni et al. 2020, 2021).

The advent of the Vera C. Rubin Observatory (Ivezic et al. 2019) presents us with a great opportunity to identify a population of kilonovae independent of any gravitational-wave or GRB trigger, thanks to the unprecedented volume that the Legacy Survey of Space and Time (LSST) will be able to probe (see, e.g., Andreoni et al. 2019; Setzer et al. 2019). Unfortunately, due to their fast-fading and intrinsically underluminous properties, “detection” is not enough; it is imperative that kilonova candidates found by the Rubin Observatory are recognized as such in real time so that follow-up observations can confirm their nature.

Projects exist that are dedicated to fast-transient discovery in current wide-field surveys such as the Zwicky Transient Facility (ZTF; Bellm et al. 2019; Graham et al. 2019). The “ZTF Realtime Search and Triggering” (“ZTFReST”,¹⁶ Andreoni et al. 2021) project, for example, employs (i) alert queries, (ii) forced point-spread-function photometry, and (iii) nightly light-curve stacking in flux space to discover fast-evolving transients such as kilonovae. ZTFReST is proving to be very effective at identifying extragalactic fast transients, having already revealed seven serendipitously discovered GRB afterglows and at least two supernova shock breakouts in 2020 and in the first three months of 2021 (Andreoni et al. 2021).

Possible cadences (in other words, observing strategies, in this context) for Rubin Observatory were accurately simulated by the LSST project using the Operations Simulator software (OpSim; Delgado et al. 2014). In the last decade, the broader astronomical community has been invited to develop “metrics” that would help in evaluating the efficacy of different cadences for specific science cases, in a quantitative way. Metrics can therefore be applied systematically to a set of cadence simulations for many science cases. In this way, results can be compared and contrasted before a final decision on the Rubin observing strategy is reached by the Survey Cadence Optimization Committee.

In this work, we used the most recent OpSim simulations and a set of new metrics to assess the effectiveness of cadence options for untriggered, or “serendipitous,” kilonova discovery.

We employed metrics that both assess Rubin Observatory’s ability to simply detect the transients, as well as metrics that are designed to identify a transient as “fast” based on its flux evolution. We argue that the latter is the most appropriate metric for potentially maximizing the science output from these rare objects, and we provide suggested cadences based on this metric.

2. Methods

We used the new `kneMetrics`¹⁷ to recover synthetic kilonova light curves injected in OpSim simulations. The synthetic light curves are taken from Dietrich et al. (2020), which rely on the radiative transfer code POSSIS (Bulla 2019), which vary four parameters over physically viable priors: the dynamic ejecta mass M_{dyn} , the disk-wind ejecta mass M_{wind} , the half-opening angle of the lanthanide-rich dynamical-ejecta component ϕ , and the viewing angle ι (see Dietrich et al. 2020 for more details about the adopted geometry). Examples of synthetic light curves injected in the Rubin baseline cadence can be found in Figure 1.

2.1. Metrics

To assess kilonova detectability in different cadence simulations, we employed a number of metrics. We improved the existing `TDEsPopMetric`, designed to inject and recover diverse populations of tidal disruption event light curves, by adding the possibility to inject synthetic transients distributed uniformly in volume (with numbers increasing as a function of distance to the third power), rather than placed at a fixed distance. Light curves at a larger distance share the same properties of those at lower distances, but their apparent luminosity is fainter, making them detectable for shorter times and only when the images’ magnitude limits are particularly deep.

The metrics most relevant to this work, all included as functions in the `kneMetrics` code, are:

1. `multi_detect`: ≥ 2 detections $> 5\sigma$;
2. `ztfrest_simple`: metric that reproduces a discovery algorithm similar¹⁸ to ZTFReST, in which sources found to be rising faster than 1 mag day^{-1} and fading faster than 0.3 mag day^{-1} are selected;
3. `ztfrest_simple_red`: same as `ztfrest_simple`, but applied only to *izy* bands;
4. `ztfrest_simple_blue`: same as `ztfrest_simple`, but applied only to *ugr* bands.

The metrics were deliberately designed to range from standard transient detection (with ≥ 2 detections), which typically provides only spatial information on the celestial coordinates of a source, to methods more likely to lead to source characterization—in other words, kilonova discovery. Simple detection can be crucial during gravitational-wave follow-up, but is of little use during fast-transient searches in the regular survey, especially for transients at large distances. Importantly, the conclusions of this study can be applied to a

¹⁷ https://github.com/LSST-nonproject/sims_maf_contrib/blob/master/mafContrib/kneMetrics.py

¹⁸ In ZTFReST, linear fitting is performed, while the `ztfrest_simple` metric relies on a more simplistic estimate of the rising or fading rates based on the time and magnitude differences between the brightest and the faintest detected ($>5\sigma$) points in the light curves.

¹⁶ github.com/growth-astro/ztfrest

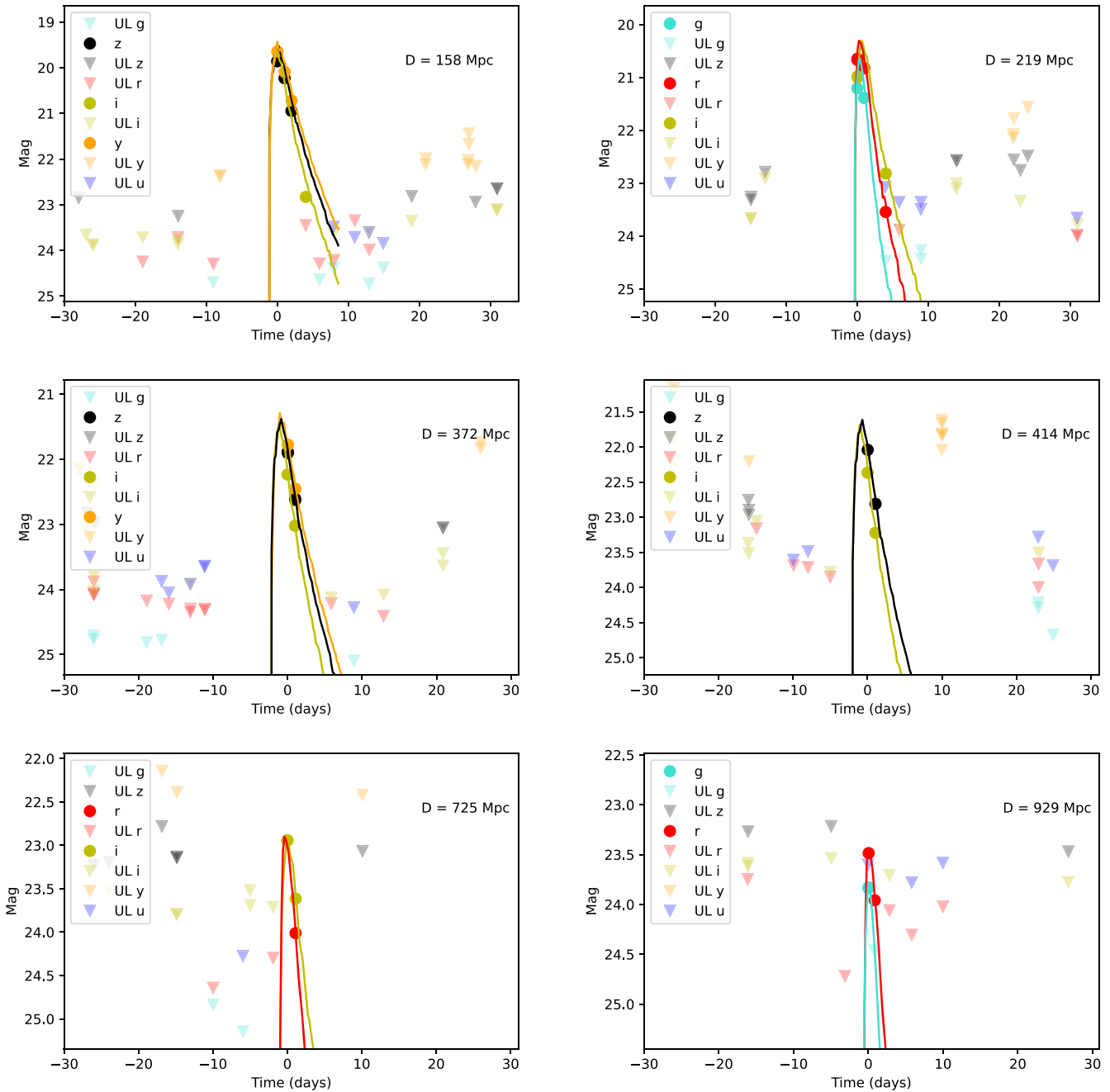


Figure 1. Examples of GW170817-like kilonova light curves injected in the baseline cadence (v1.7, individual exposures). Observations from 30 days before peak to 30 days after peak are presented. The light curves were uniformly distributed in volume and uniformly distributed in time throughout the 10 yr survey. Circles indicate the detections, solid lines show the simulated light curves in bands where at least one detection is present, and triangles indicate 5σ upper limits. The luminosity distance at which each light curve is placed is also indicated.

range of fast transients, including, for example, GRB afterglows and fast blue optical transients, for which light-curve sampling with spacing between 1 hr and 1 day is crucial.

There are a variety of methods in the literature to promptly identify fast-transient candidates. For example, methods are being developed for early transient classification via machine-learning techniques (e.g., Muthukrishna et al. 2019), or as part of the Photometric LSST Astronomical Time Series Classification Challenge (Kessler et al. 2019). Prior work on detecting and identifying fast transients in Rubin LSST Opsims includes Bianco et al. (2019). A simple but effective strategy to identify transients with rapidly fading or rising light curves can be based

on magnitude rise- and decay-rate measurements. In this work, we consider significant fading rates to be those faster than 0.3 mag day^{-1} , which is the threshold used in real time by the ZTFReST pipeline and is expected to be particularly suitable for the discovery of kilonovae from BNS mergers (Figure 2), or rising rates faster than 1 mag day^{-1} , which can separate rapidly evolving transients from most supernovae. Within ZTFReST, this has greatly helped to separate fast-transient candidates from slower, “contaminant” sources, with $\sim 30\%$ purity in “archival” data searches when considering only fade rates and thresholds tailored for each band.

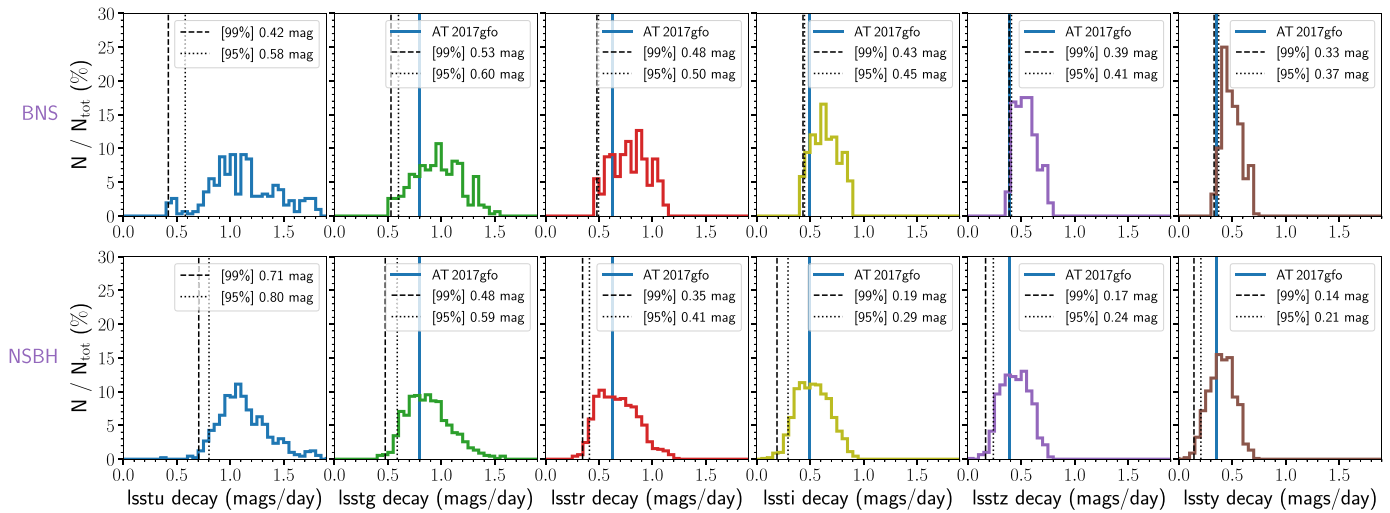


Figure 2. A distribution of fade rates was calculated using the kilonova model grid obtained by Bulla (2019), tailored for BNS (upper panels) and NSBH mergers (lower panels). Averaged decay rates from peak to 6 days later are shown in Rubin *ugrizy* bands from left to right. Dashed and dotted–dashed vertical lines indicate the lower 99% and 95% decay rates for each distribution. Blue vertical lines indicate the decay rates for the GW170817 kilonova in each band. A fading-rate threshold of 0.3 mag day^{-1} can enable the identification of kilonovae from BNS mergers ($>99\%$ of the distribution) in all filters.

2.2. Kilonova Models

In this work, we considered kilonova models from the grid generated with the three-dimensional radiation transfer simulation code POSSIS (Bulla 2019). The model grid allowed us to explore a diversity of intrinsic properties, such as ejecta masses, as well as different viewing angles to the system.

First, we injected synthetic light curves using a single model: the GW170817-like kilonova (dynamical-ejecta mass $M_{\text{dyn}} = 0.005M_{\odot}$, disk-wind mass $M_{\text{wind}} = 0.050M_{\odot}$, and viewing angle $\iota = 25.8^{\circ}$). A half-opening angle $\phi = 30^{\circ}$ for the lanthanide-rich region is used for this model and all the other models considered in this work. Second, we injected a population of kilonovae with the same ejecta masses of the GW170817-like model but viewed from 11 viewing angles, uniformly distributed in $\cos(\iota)$. Third, we explored kilonova detectability in an optimistic and a pessimistic scenarios, in which the kilonova properties make it particularly bright or dim, respectively. Ejecta masses were chosen to be physically realistic as determined by numerical relativity simulations, with $M_{\text{dyn}} = 0.020M_{\odot}$, $M_{\text{wind}} = 0.090M_{\odot}$ for the optimistic scenario, and $M_{\text{dyn}} = 0.005M_{\odot}$, $M_{\text{wind}} = 0.010M_{\odot}$ for the pessimistic scenario.

3. Results

3.1. GW170817-like Kilonova Light Curves

Cadences were made available in several releases and were grouped into “families”, in which ideas that deviate from the baseline cadence were implemented and encompass parameter variations, for example in the area of the footprint. Detailed information about simulations can be found in official Rubin Observatory online resources.¹⁹

Figure 3 shows results obtained by injecting 5×10^5 synthetic GW170817-like kilonova light curves, uniformly distributed in volume out to a luminosity distance of 1.5 Gpc, in OpSim simulated cadences part of the v1.5²⁰

(bottom panels) and v1.7²¹ and v1.7.1²² releases (top panels). In all panels of Figure 3, each point indicates the ratio between the mean recovery fraction of an individual cadence and the maximum recovery fraction of the baseline cadence that returned the most kilonova detections. Results from those simulations are grouped by cadence family, such that all the results from cadences belonging to a certain family line up at the same abscissa. The maximum and minimum normalized recovery fractions for each family are marked by red and black triangles, respectively, and the mean recovery fraction for each cadence family is indicated by a blue circular marker to guide the eye. The results displayed in Figure 3 were obtained using the `multi_detect` (right panels) and the `ztfrest_simple` (left panels) metrics described in Section 2.1.

In all simulations, the best baseline cadence entails individual 30 s exposures (`baseline_nexp1`). The baseline cadence with $2 \times 15 \text{ s}$ snaps (`baseline_nexp2`) performs consistently worse. The number of recovered kilonovae in cadence families simulated as part of the v1.5 cadence release (bottom panels) are relatively similar, with results comparable with the best baseline cadence within 15%. When looking at v1.7 cadences, it is evident that the best baseline performs distinctly better than any other cadence in terms of kilonova detection (`multi_detect` metric; top-right panel of Figure 3). The baseline cadence does a better job than most cadence families, also according to the `ztfrest_simple` metric. We found that rolling cadences, in which a smaller fraction of the footprint is observed in each season at higher cadence, perform significantly ($\sim 50\%$ – 60%) worse as coded for the v1.7 release than the baseline cadence.²³ However, rolling cadences as part of the v1.7.1 release, indicated as “new_rolling” in the figure, perform up to $\sim 20\%$ better than the baseline cadence (in the figure, uncertainties are in the order of 5%–10%). In order to compare baseline and rolling cadences

²¹ https://github.com/lstt-sims/sims_featureScheduler_runs1.7

²² <https://community.lsst.org/t/survey-simulations-v1-7-1-release-april-2021/4865>

²³ Significant changes to the OpSim approach to simulate rolling-cadence strategies were implemented for v1.7, such that these simulations should be considered more reliable (see Bianco et al. 2022).

¹⁹ E.g., https://github.com/lstt-pst/survey_strategy.

²⁰ https://github.com/lstt-sims/sims_featureScheduler_runs1.5

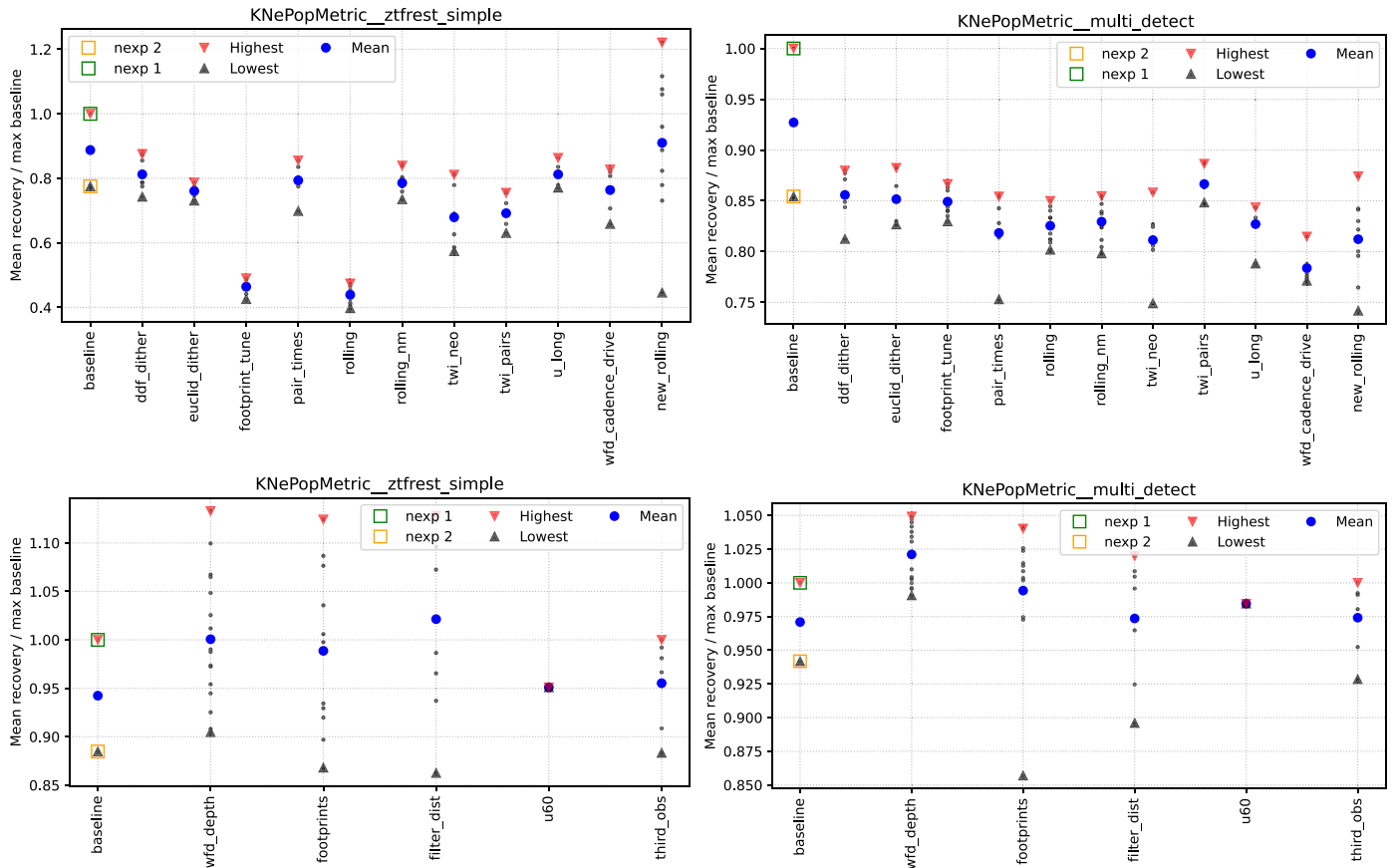


Figure 3. For each cadence family, we report the ratio between the recovery fraction of the individual cadences and the maximum recovery fraction from the best baseline cadence (baseline_nexp1). Blue dots indicate the mean of the cadences’ recovery fractions, red triangles their maximum, and black triangles their minimum. The two-snaps baseline cadence (baseline_nexp2) performs systematically worse than the single-exposure baseline cadence. Simulations part of FBS v1.7 (top) and of FBS v1.5 (bottom) are considered separately.

with a higher statistical significance, we ran simulations in which the number of injected sources was increased to 10^6 , using a variety of surrogate models. A summary of the results can be found in Table 1.

When we injected GW170817-like kilonovae, the baseline cadence performed better than the best rolling cadence²⁴ at any distance with the `multi_detect` metric (Figure 4, central panel), but the rolling cadence outperforms the baseline cadence beyond ~ 400 Mpc with the `ztfrest_simple` metric. This means that a rolling cadence could enable the identification of a few more kilonova candidates than the baseline cadence at large distances. In total, 32–334 kilonovae can be expected to be detectable with the baseline cadence and 23–238 with the rolling cadence, assuming that all kilonovae are similar to the observed GW170817. However, the number of kilonovae recognizable to be fast transients (`ztfrest_simple` metric) would be 3–29 and 3–32 for the baseline and rolling cadences, respectively.

Nearby kilonovae have the potential to be recognized sooner, associated with hosts at known redshifts, and can be better characterized with follow-up observations than distant (fainter) sources. To better explore detectability of nearby kilonovae, we injected 10^6 GW170817-like kilonovae uniformly distributed in volume out to 300 Mpc, which is within the distance range where the best Wide Fast Deep (WFD) baseline cadence performs better than any of the rolling cadences simulated so

far. With the best baseline cadence, we can expect up to 101 kilonovae to be detectable at at least twice in this distance range and up to 31 could be recognized to be fast-fading in at least one band. In the simulations, about 68% of kilonovae were found to be fast-fading in red `izy` bands (`ztfrest_simple_red` metric) and 44% in blue `ugr` bands (`ztfrest_simple_blue` metric). Only 37% of kilonovae found in `izy` bands were detected at least four times in `ugr` bands (Figure 4, bottom panel). The combination of transient detection, color information, and possible association with a cataloged nearby galaxy (which enables an estimate of the transient’s absolute magnitude, expected to be fainter than $M \sim -16$ for most kilonovae) can lead to the identification of solid kilonova candidates. For the fraction of events that are relatively nearby (below 300 Mpc), they can be followed up spectroscopically with $\gtrsim 8$ m class telescopes such as the Very Large Telescope, Gemini, Keck, or with the upcoming SoXS at ESO New Technology Telescope (NTT), which was designed specifically for LSST transient classification, to be classified (Schipani et al. 2016). In summary, our analysis suggests that employing more observations in redder bands is preferred to maximize scientific return.

3.2. Exploring the Kilonova Light-curve Parameter Space

Multimessenger observations of GW170817 constrained the viewing angle to be $\iota = 32^{+10}_{-13}$ (Finstad et al. 2018, see also Dhawan et al. 2020). Superluminal motion from radio

²⁴ `six_stripe_scale0.90_nslc6_fpw0.9_nrw0.0v1.7_10yrs`.

Table 1
Kilonova Recovery Efficiencies (ϵ), Calculated with a Number of Metrics, for the Best Baseline Cadence and the Best Rolling Cadence

Kilonova Model	Metric	$\epsilon_{\text{Baseline}}$ ($\times 10^4$)	$\epsilon_{\text{Rolling}}$ ($\times 10^4$)	N_{KN} Baseline	N_{KN} Rolling	$N_{\text{KN,min}}$ Baseline	$N_{\text{KN,min}}$ Rolling	$N_{\text{KN,max}}$ Baseline	$N_{\text{KN,max}}$ Rolling
GW170817	multi_detect	60.5 ± 0.8	43.1 ± 0.7	130	93	32	23	334	238
$M_{\text{dyn}} = 0.005M_{\odot}$	blue_color_detect	6.8 ± 0.3	6.4 ± 0.2	15	14	4	3	38	36
$M_{\text{wind}} = 0.050M_{\odot}$	red_color_detect	2.9 ± 0.2	3.1 ± 0.2	6	7	1	2	17	18
	ztfrest_simple	5.2 ± 0.2	5.6 ± 0.2	11	12	3	3	29	32
	ztfrest_simple_blue	3.8 ± 0.2	4.4 ± 0.2	8	9	2	2	22	25
	ztfrest_simple_red	1.7 ± 0.1	2.1 ± 0.1	4	4	1	1	10	12
GW170817 <300 Mpc	multi_detect	1306.3 ± 3.6	931.2 ± 3.0	40	28	10	7	101	72
	blue_color_detect	141.0 ± 1.2	143.8 ± 1.2	4	4	1	1	11	11
	red_color_detect	369.5 ± 1.9	312.0 ± 1.8	11	10	3	2	29	24
	ztfrest_simple	400.3 ± 2.0	334.1 ± 1.8	12	10	3	3	31	26
	ztfrest_simple_blue	176.7 ± 1.3	173.0 ± 1.3	5	5	1	1	14	13
	ztfrest_simple_red	272.9 ± 1.6	244.5 ± 1.6	8	7	2	2	21	19
GW170817 viewing angles	multi_detect	31.8 ± 0.6	22.7 ± 0.5	68	49	17	12	176	127
	blue_color_detect	3.4 ± 0.2	3.4 ± 0.2	7	7	2	2	20	19
	red_color_detect	1.4 ± 0.1	1.7 ± 0.1	3	4	1	1	8	10
	ztfrest_simple	2.6 ± 0.2	2.9 ± 0.2	6	6	1	1	15	17
	ztfrest_simple_blue	1.8 ± 0.1	2.3 ± 0.1	4	5	1	1	10	13
	ztfrest_simple_red	1.0 ± 0.1	1.1 ± 0.1	2	2	0	1	6	7
Pessimistic $M_{\text{dyn}} = 0.005M_{\odot}$ $M_{\text{wind}} = 0.010M_{\odot}$	multi_detect	8.9 ± 0.3	6.5 ± 0.2	19	14	5	3	50	37
	blue_color_detect	0.8 ± 0.1	0.9 ± 0.1	2	2	0	0	5	5
	red_color_detect	0.3 ± 0.1	0.4 ± 0.1	1	1	0	0	2	3
	ztfrest_simple	0.5 ± 0.1	0.6 ± 0.1	1	1	0	0	3	4
	ztfrest_simple_blue	0.4 ± 0.1	0.4 ± 0.1	1	1	0	0	2	2
	ztfrest_simple_red	0.2 ± 0.1	0.3 ± 0.1	0	1	0	0	1	2
Optimistic $M_{\text{dyn}} = 0.020M_{\odot}$ $M_{\text{wind}} = 0.090M_{\odot}$	multi_detect	116.6 ± 1.1	87.0 ± 0.9	251	187	62	46	641	479
	blue_color_detect	11.9 ± 0.3	12.9 ± 0.4	26	28	6	7	67	72
	red_color_detect	5.2 ± 0.2	5.9 ± 0.2	11	13	3	3	29	34
	ztfrest_simple	9.2 ± 0.3	10.8 ± 0.3	20	23	5	6	52	61
	ztfrest_simple_blue	6.7 ± 0.3	8.3 ± 0.3	14	18	3	4	38	47
	ztfrest_simple_red	3.2 ± 0.2	4.2 ± 0.2	7	9	2	2	18	24

Note. The efficiency was then converted into the number of expected kilonovae using the BNS merger rate $R = 320_{-240}^{+490} \text{ Gpc}^{-3} \text{ yr}^{-1}$ from the GWTC-2 catalog (The LIGO Scientific Collaboration et al. 2021), where N_{KN} corresponds to the median rate and $N_{\text{KN,min}}$, $N_{\text{KN,max}}$ correspond to the 90% symmetric credible intervals, taking the uncertainty in ϵ into account. A duration of 10 yr for the WFD survey was assumed.

observations suggests a lower value for the viewing angle of about 15° – 20° (Mooley et al. 2018; Ghirlanda et al. 2019).

However, merging BNS systems can be oriented in any direction with respect to the observer. We also compared the performance of baseline and rolling cadences by injecting synthetic light curves, from the grid of kilonova models simulated with POSSIS, with the same intrinsic parameters as the GW170817-like model (Section 2.2), but at different viewing angles. According to our simulations, up to 15 (17) kilonovae should be identified as fast transients in the baseline (rolling) cadence, while up to 176 (127) kilonovae should be detectable at least twice.

Finally, we assessed kilonova detectability for “pessimistic” and “optimistic” kilonova models, in which the ejecta masses make the optical emission particularly faint or bright (see Section 2.2). For the pessimistic case, only a handful of kilonovae are expected to be present in Rubin images, with at most five kilonovae expected to be recognizable as fast transients. On the other hand, the optimistic scenario could result in >50 kilonovae found to evolve rapidly with the baseline cadence and >60 with the currently best rolling cadence. A better understanding of the kilonova luminosity function is required to set more precise serendipitous kilonova discovery expectations.

3.3. Comparison with Other Work

Our results can be compared with a sample of related work on prospects for serendipitous detection of kilonovae by the Rubin Observatory. One difference tends to be, in some cases, the BNS merger rate assumed, for example, $R = 10^3 \text{ Gpc}^{-3} \text{ yr}^{-1}$ (e.g., Scolnic et al. 2018; Setzer et al. 2019) was adopted, or up to $R = 1.5 \times 10^3 \text{ Gpc}^{-3} \text{ yr}^{-1}$ (Cowperthwaite et al. 2019). These rates were consistent with gravitational-wave observations before the third LIGO–Virgo–KAGRA observing run (O3), but is larger than the upper bound of the most recent rate from the GWTC-2 catalog, used in this work, of $810 \text{ Gpc}^{-3} \text{ yr}^{-1}$ (The LIGO Scientific Collaboration et al. 2021). We also caution that the newer simulated cadences underwent some changes with respect to those available in 2018.

For a uniform population of GW170817-like kilonovae, Setzer et al. (2019) expect about 58 kilonovae to be detected during the survey using the selection criteria developed by Scolnic et al. (2018), which aim at identifying transients with multiband detections that evolve faster than most supernovae. Those results, rescaled to a lower BNS merger rate, lie well within the range of 32–334 kilonovae that could be found with the looser `multi_detect` metric, while they exceed the expected 3–29 kilonovae that could be found to be rapidly

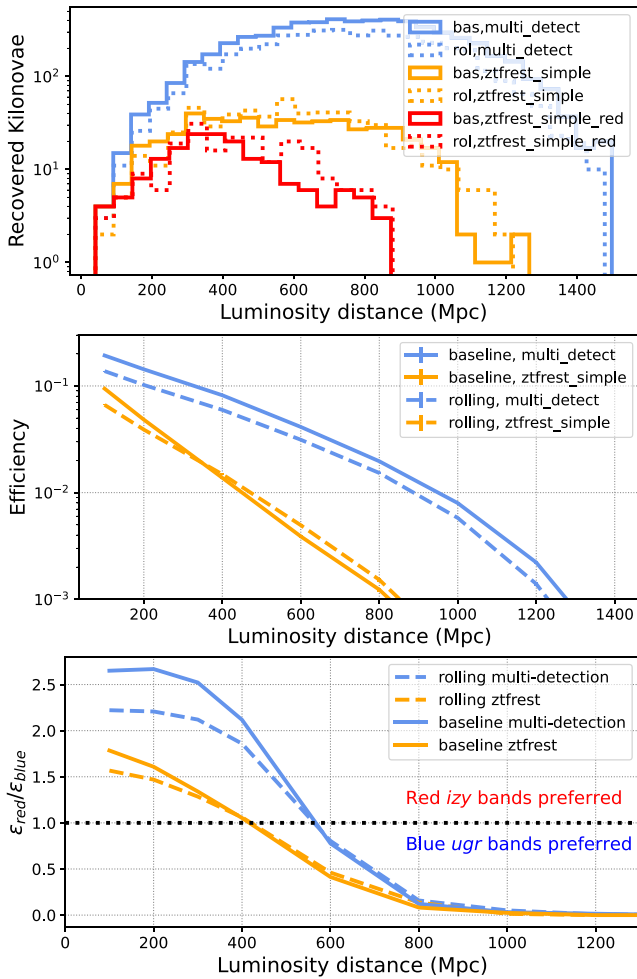


Figure 4. Top: Distribution of recovered kilonovae using a simple multi-detection metric (cyan), a ZTFReST-like metric (orange), and a ZTFReST-like metric applied only to red (*izy*) bands (red line). One million sources were injected in a uniform distribution in a volume between 10 Mpc and 1.5 Gpc. Center: Efficiency as a function of luminosity distance; 5×10^5 sources were injected at regular intervals. For the *ztfrest_simple* metric, due to the rapidly growing rate at the edge of the sensitive volume, small differences between detection efficiencies for the rolling and the baseline cadence beyond ~ 400 Mpc are enough to yield an improvement of $\sim 20\%$ in kilonova detection. Bottom: Ratio between the detection efficiency in redder *izy* bands and in bluer *ugr* bands for multidetection and ZTFReST-like metrics. Employing redder filters presents clear advantages at lower distances, where spectroscopic and multiwavelength follow-up observations are possible.

evolving with the stricter *ztfrest_simple* metric. The ~ 27 expected kilonova detections from a representative population of BNS mergers in the baseline cadence, corrected for the merger rate, lies between the results that we obtained for pessimistic and optimistic kilonova models with the *ztfrest_simple* metric. Overall, our *ztfrest_simple* metric results are closer to those obtained by Cowperthwaite et al. (2019), who employed stricter selection criteria than Scolnic et al. (2018) and Setzer et al. (2019). This highlights the importance of realistic filters when estimating expected rates.

4. Conclusion

Rubin Observatory has great potential for revealing a population of kilonovae during the WFD survey, in addition to discoveries made following up gravitational-wave triggers. We injected synthetic kilonova light curves into simulated

Rubin observations to assess which ones of the available cadences can maximize serendipitous kilonova discovery. We demonstrated that, for the WFD survey, the simulated baseline cadence with single 30 s exposures should be greatly preferred over 2×15 s consecutive snaps for kilonova discovery.

Rolling cadences are expected to be particularly suitable for fast-transient discovery (e.g., Andreoni et al. 2019; Setzer et al. 2019). We found that the development of rolling cadences has significantly improved from OpSim version v1.7 to v1.7.1. While this indicates progress, the baseline plan may still be preferred over any other cadence family currently available due to a larger efficiency at detecting more nearby (and therefore brighter) fast transients that are easier to follow-up and classify with other telescopes. We recommend simulating new rolling cadences by further optimizing the algorithms used in v1.7.1, possibly maximizing the exposure time in each band (barring the *u* band) rather than using snap pairs.

We found strong evidence that red *izy* bands are preferred for kilonova discovery at distances below 300 Mpc, in agreement with the results of other studies such as, for example, Almualla et al. (2021) and Sagués Carracedo et al. (2021). This is expected because kilonovae appear as red and rapidly reddening transients due to heavy *r*-process elements synthesized in neutron-rich ejecta. At redder wavelengths, kilonova light curves can be brighter and longer lived, especially if the system is viewed from equatorial viewing angles (e.g., Bulla 2019). Very rapid “blue” kilonovae could be found at larger distances (Figure 4) due to the greater sensitivity of the *g* and *r* filters, however, these kilonovae might be rarer and more difficult to classify spectroscopically. Therefore, we recommend that the number of *izy* observations is increased in the WFD cadence plan. Such red-band observations would be particularly effective, scientifically, if coupled with at least one observation in the *g* (preferred) or *r* bands on the same night, so that kilonovae can be separated photometrically from other transients and their temperature evolution can be measured. A recommendation for same-night multiband photometry in LSST has already been put forward, for example by Andreoni et al. (2019), Bianco et al. (2019), and Setzer et al. (2019). In particular, Bianco et al. (2019) address the advantages of acquiring sets of three exposures per field in the same night, in two filters and appropriately spaced in time, toward rapid identification of rare fast transients.

Major uncertainty in the results of this work results from our limited understanding of the BNS merger rate and the kilonova luminosity function. Systematic kilonova searches during gravitational-wave follow-up (e.g., Kasliwal et al. 2020), short GRB follow-up (e.g., Gompertz et al. 2018; Rossi et al. 2020), and untriggered wide-field surveys (e.g., Doctor et al. 2017; Andreoni et al. 2020, 2021; McBrien et al. 2021) are expected to improve those measurements significantly before Rubin Observatory’s first light.

We thank Peter Yoachim and Lynne Jones. We thank the anonymous referee for comments and suggestions that improved the manuscript. This paper was created in the nursery of the Rubin LSST Transient and Variable Star Science Collaboration.²⁵ The authors acknowledge the support of the Vera C. Rubin Legacy Survey of Space and Time Transient and Variable Stars Science Collaboration that provided

²⁵ <https://lsst-tvssc.github.io/>


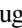









opportunities for collaboration and exchange of ideas and knowledge and of Rubin Observatory in the creation and implementation of this work. The authors acknowledge the support of the LSST Corporation, which enabled the organization of many workshops and hackathons throughout the cadence optimization process by directing private funding to these activities.

M.W.C acknowledges support from the National Science Foundation with grant No. PHY-2010970. M.B. acknowledges support from the Swedish Research Council (Reg. No. 2020-03330). A.G, A.S.C, and E.C.K. acknowledge support from the G.R.E.A.T. research environment funded by *Vetenskapsrådet*, the Swedish Research Council, under project No. 2016-06012, and support from The Wenner-Gren Foundations. This work was supported by the Preparing for Astrophysics with LSST Program, funded by the Heising Simons Foundation through grant 2021-2975, and administered by Las Cumbres Observatory.

This research uses services or data provided by the Astro Data Lab at NSF's National Optical-Infrared Astronomy Research Laboratory. NOIRLab is operated by the Association of Universities for Research in Astronomy (AURA), Inc. under a cooperative agreement with the National Science Foundation.

Software: LSST metrics analysis framework (MAF; Jones et al. 2014); Astropy (Astropy Collaboration et al. 2013); JupyterHub.²⁶

ORCID iDs

Igor Andreoni  <https://orcid.org/0000-0002-8977-1498>
 Michael W. Coughlin  <https://orcid.org/0000-0002-8262-2924>
 Eric C. Bellm  <https://orcid.org/0000-0001-8018-5348>
 Federica B. Bianco  <https://orcid.org/0000-0003-1953-8727>
 Mattia Bulla  <https://orcid.org/0000-0002-8255-5127>
 Tim Dietrich  <https://orcid.org/0000-0003-2374-307X>
 Ariel Goobar  <https://orcid.org/0000-0002-4163-4996>
 Erik C. Kool  <https://orcid.org/0000-0002-7252-3877>
 Xiaolong Li  <https://orcid.org/0000-0002-0514-5650>
 Fabio Ragosta  <https://orcid.org/0000-0003-2132-3610>
 Leo P. Singer  <https://orcid.org/0000-0001-9898-5597>

References

- Abbott, B. P., Abbott, R., Abbott, T. D., et al. 2017a, *Natur*, 551, 85
 Abbott, B. P., Abbott, R., Abbott, T. D., et al. 2017b, *PhRvL*, 119, 161101
 Almualla, M., Anand, S., Coughlin, M. W., et al. 2021, *MNRAS*, 504, 2822
 Andreoni, I., Ackley, K., Cooke, J., et al. 2017, *PASA*, 34, e069
 Andreoni, I., Anand, S., Bianco, F. B., et al. 2019, *PASP*, 131, 068004
 Andreoni, I., Coughlin, M. W., Kool, E. C., et al. 2021, *ApJ*, 918, 63
 Andreoni, I., Kool, E. C., Sagués Carracedo, A., et al. 2020, *ApJ*, 904, 155
 Annala, E., Gorda, T., Kurkela, A., & Vuorinen, A. 2018, *PhRvL*, 120, 172703
 Arcavi, I., Hosseinzadeh, G., Howell, D. A., et al. 2017, *Natur*, 551, 64
 Astropy Collaboration, Robitaille, T. P., Tollerud, E. J., et al. 2013, *A&A*, 558, A33
 Baker, T., Bellini, E., Ferreira, P. G., et al. 2017, *PhRvL*, 119, 251301
 Barnes, J., & Kasen, D. 2013, *ApJ*, 775, 18
 Barnes, J., Kasen, D., Wu, M.-R., & Martínez-Pinedo, G. 2016, *ApJ*, 829, 110
 Bauswein, A., Goriely, S., & Janka, H.-T. 2013, *ApJ*, 773, 78
 Bellm, E. C., Kulkarni, S. R., Graham, M. J., et al. 2019, *PASP*, 131, 018002
 Berger, E., Fong, W., & Chornock, R. 2013, *ApJL*, 774, L23
 Bianco, F. B., Drout, M. R., Graham, M. L., et al. 2019, *PASP*, 131, 068002
 Bianco, F. B., Ivezić, Ž., Jones, R. L., et al. 2022, *ApJS*, 258, 1
 Blinnikov, S. I., Novikov, I. D., Perevodchikova, T. V., & Polnarev, A. G. 1984, *SvAL*, 10, 177
 Bulla, M. 2019, *MNRAS*, 489, 5037
 Capano, C. D., Tews, I., Brown, S. M., et al. 2020, *NatAs*, 4, 625
 Coughlin, M. W., Dietrich, T., Heinzel, J., et al. 2020, *PhRvR*, 2, 022006
 Coulter, D. A., Foley, R. J., Kilpatrick, C. D., et al. 2017, *Sci*, 358, 1556
 Cowperthwaite, P. S., Berger, E., Villar, V. A., et al. 2017, *ApJL*, 848, L17
 Cowperthwaite, P. S., Villar, V. A., Scolnic, D. M., & Berger, E. 2019, *ApJ*, 874, 88
 Delgado, F., Saha, A., Chandrasekharan, S., et al. 2014, *Proc. SPIE*, 9150, 915015
 Dhawan, S., Bulla, M., Goobar, A., Sagués Carracedo, A., & Setzer, C. N. 2020, *ApJ*, 888, 67
 Dietrich, T., Coughlin, M. W., Pang, P. T. H., et al. 2020, *Sci*, 370, 1450
 Dietrich, T., & Ujevic, M. 2017, *CQGra*, 34, 105014
 Doctor, Z., Kessler, R., Chen, H. Y., et al. 2017, *ApJ*, 837, 57
 Essick, R., Landry, P., & Holz, D. E. 2020, *PhRvD*, 101, 063007
 Ezquiaga, J. M., & Zumalacárregui, M. 2017, *PhRvL*, 119, 251304
 Fernández, R., Kasen, D., Metzger, B. D., & Quataert, E. 2015, *MNRAS*, 446, 750
 Fernández, R., Tchekhovskoy, A., Quataert, E., Foucart, F., & Kasen, D. 2019, *MNRAS*, 482, 3373
 Finstad, D., De, S., Brown, D. A., Berger, E., & Biwer, C. M. 2018, *ApJL*, 860, L2
 Fishbach, M., Gray, R., Magaña Hernandez, I., et al. 2019, *ApJL*, 871, L13
 Ghirlanda, G., Salafia, O. S., Paragi, Z., et al. 2019, *Sci*, 363, 968
 Gompertz, B. P., Levan, A. J., Tanvir, N. R., et al. 2018, *ApJ*, 860, 62
 Graham, M. J., Kulkarni, S. R., Bellm, E. C., et al. 2019, *PASP*, 131, 078001
 Hotokezaka, K., Kiuchi, K., Kyutoku, K., et al. 2013, *PhRvD*, 87, 024001
 Hotokezaka, K., Nakar, E., Gottlieb, O., et al. 2019, *NatAs*, 3, 940
 Ivezić, Ž., Kahn, S. M., Tyson, J. A., et al. 2019, *ApJ*, 873, 111
 Jin, Z.-P., Covino, S., Liao, N.-H., et al. 2020, *NatAs*, 4, 77
 Jones, R. L., Yoachim, P., Chandrasekharan, S., et al. 2014, *Proc. SPIE*, 9149, 91490B
 Kasen, D., Badnell, N. R., & Barnes, J. 2013, *ApJ*, 774, 25
 Kasen, D., Metzger, B., Barnes, J., Quataert, E., & Ramirez-Ruiz, E. 2017, *Natur*, 551, 80
 Kasliwal, M. M., Anand, S., Ahumada, T., et al. 2020, *ApJ*, 905, 145
 Kasliwal, M. M., Nakar, E., Singer, L. P., et al. 2017, *Sci*, 358, 1559
 Kessler, R., Narayan, G., Avelino, A., et al. 2019, *PASP*, 131, 094501
 Lamb, G. P., Tanvir, N. R., Levan, A. J., et al. 2019, *ApJ*, 883, 48
 Lattimer, J. M., & Schramm, D. N. 1974, *ApJL*, 192, L145
 Li, L.-X., & Paczyński, B. 1998, *ApJL*, 507, L59
 McBrien, O. R., Smartt, S. J., Huber, M. E., et al. 2021, *MNRAS*, 500, 4213
 Metzger, B. D. 2017, arXiv:1710.05931
 Metzger, B. D., Piro, A. L., & Quataert, E. 2008, *MNRAS*, 390, 781
 Mooley, K. P., Deller, A. T., Gottlieb, O., et al. 2018, *Natur*, 561, 355
 Most, E. R., Weih, L. R., Rezzolla, L., & Schaffner-Bielich, J. 2018, *PhRvL*, 120, 261103
 Muthukrishna, D., Narayan, G., Mandel, K. S., Biswas, R., & Hložek, R. 2019, *PASP*, 131, 118002
 Perley, D. A., Metzger, B. D., Granot, J., et al. 2009, *ApJ*, 696, 1871
 Pian, E., D'Avanzo, P., Benetti, S., et al. 2017, *Natur*, 551, 67
 Radice, D., & Dai, L. 2019, *EPJA*, 55, 50
 Radice, D., Perego, A., Zappa, F., & Bernuzzi, S. 2018, *ApJL*, 852, L29
 Rossi, A., Stratta, G., Maiorano, E., et al. 2020, *MNRAS*, 493, 3379
 Sagués Carracedo, A., Bulla, M., Feindt, U., & Goobar, A. 2021, *MNRAS*, 504, 1294
 Schipani, P., Claudi, R., Campana, S., et al. 2016, *Proc. SPIE*, 9908, 990841
 Scolnic, D., Kessler, R., Brout, D., et al. 2018, *ApJL*, 852, L3
 Setzer, C. N., Biswas, R., Peiris, H. V., et al. 2019, *MNRAS*, 485, 4260
 Siegel, D. M., & Metzger, B. D. 2018, *ApJ*, 858, 52
 Smartt, S., Chen, T.-W., Jerkstrand, A., et al. 2017, *Natur*, 551, 75
 Tanvir, N., Levan, A., Fruchter, A., et al. 2013, *Natur*, 500, 547
 Tews, I., Margueron, J., & Reddy, S. 2018, *PhRvC*, 98, 045804
 The LIGO Scientific Collaboration, The Virgo Collaboration, Abbott, R., et al. 2021, *ApJL*, 913, L7

²⁶ <https://jupyterhub.readthedocs.io/en/stable/index.html>